International Journal of Pattern Recognition and Artificial Intelligence

Identification of brain functional networks using a model-based approach

Vangelis P. Oikonomou

Information Technologies Institute, Centre for Research and Technology Hellas, CERTH-ITI, 6th km Charilaou-Thermi Road, 57001 Thermi-Thessaloniki, Greece, viknmu@iti.gr

Konstantinos Blekas

Department of Computer Science, University of Ioannina, 45110 Ioannina, Greece, kblekas@cs.uoi.gr

Loukas Astrakas

Medical School, University of Ioannina, 45110 Ioannina, Greece, astrakas@uoi.gr

Functional MRI (fMRI) is a valuable brain imaging technique. A significant problem, when analyzing fMRI time series, is the finding of functional brain networks when the brain is at rest, i.e., no external stimulus is applied to the subject. In this work we present a probabilistic method to estimate the Resting State Networks (RSNs) using a model-based approach. More specifically, RSNs are assumed to be the result of a clustering procedure. In order to perform the clustering, mixture of regression models are used. Furthermore, special care has been given in order to incorporate important functionalities, such as spatial and embedded sparsity enforcing properties, through the use of informative priors over the model parameters. Another interesting feature of the proposed scheme is the flexibility to handle all the brain time series at once, allowing more robust solutions. We provide comparative experimental results, using an artificial fMRI dataset and two real resting state fMRI datasets, that empirically illustrate the efficiency of the proposed regression mixture model.

Keywords: fMRI data analysis; Resting State Networks; Regression mixture models; MRF prior; Sparseness

1. Introduction

fMRI is a brain imaging technique describing the function of the brain by using task - based (or stimulus driven) paradigms. This is accomplished by measuring the relative change of the MRI signal from the baseline (a.k.a. BOLD signal) during the performance of a task or in response to a stimulus. Besides task-based paradigms, fMRI technique can be used to examine the brain when the subject does not perform any specific task (i.e. is at rest). This approach is called resting state fMRI and it investigates the temporal correlation of fMRI time series between distinct spatially regions in order to identify RSNs. A significant property of RSNs is that the most valuable information of BOLD time series is concentrated on low frequencies. The

importance of these low frequency fluctuations was first reported by [5].

Brain imaging studies have reveal consistent spatial patterns of human brain using both fMRI [5] and positron emission tomography (PET)[35]. These patterns have been termed as "resting-state networks" (RSNs)[15,2] or as "intrinsic connectivity networks"[34]. In the literature a large number of RSNs have been reported, where the Default Mode Network (DMN) is the most significant. Studies have shown that brain areas within the DMN play a significant role to the overall function of the brain. More specifically, it has been observed that connections between brain areas belonging in the same network are disrupted in pathological cases such as Alzheimer disease [22]. Several other RSNs have also been identified. They include the somatosensory network, the visual network and the auditory network among others [9]. These networks have demonstrated high consistency and reproducibility across subjects. Furthermore, they have been used to study Alzheimer's disease[16], schizophrenia[17], lateral sclerosis[44] and Attention Deficit Hyperactivity Disorder (ADHD)[32].

The methods related to the analysis of resting state fMRI data are divided into two general groups: model-driven methods and model-free (or data-driven) methods [20]. At first, model-based methods have been applied to analyze the functional connectivity of the brain through fMRI data. In [5] a method, using seeds from specific brain regions, was proposed to derive a model for data analysis. This method defines a priori a voxel, or a region of interest (ROI) in order to to build a model for time series analysis (used as a regressor in a linear correlation analysis, or as a general linear model when confounding effects are used in the analysis). An extension was the adoption of the cross-correlation metric to deal with lags [7], as well as the use of coherence [37] for capturing the properties of frequency domain. The selection of a seed region presents a substantial drawback of seed-based approach which may bias the results. However, careful selection of seed regions could provided interesting results [15,34,40].

A commonly used model-free method to analyse fMRI data is the Independent Component Analysis (ICA). ICA was first applied to fMRI data collected during an experimental task [25] and later it was applied to resting-state fMRI data [18,2]. The RSNs derived from ICA present consistency across participants and scan sessions[9], while the method has been widely used to study clinical populations (e.g. Alzheimer's disease[16], schizophrenia[17], lateral sclerosis[44]). The aim of ICA is to decompose a two-dimensional data matrix into the time courses and the spatial independent maps. ICA assumes that a fMRI data set consists of a mix of independent signals from a number of spatially distributed sources, and decomposes the data into several such independent components. ICA estimates component maps of maximal spatial independence (from each other), however, this does not preclude spatial overlap between components [2]. A major drawback of ICA is the specification of the number of components. Although methods for the estimation of this number are provided with various ICA toolboxes, in practice this number is provided by the

user [8,24]. Furthermore, ICA analysis does not provide naturally an inference mechanism. Although several ICA analysis methods have been proposed in the literature, this issue remains an obstacle on the identification of brain models. Similar to ICA approach, Dictionary Learning (DL) approaches factorize the data matrix by an over-complete dictionary basis matrix and a reference weight matrix via an effective online dictionary learning algorithm [14,45,23]. However, the difference between the two approaches lay on the underlying assumption that govern the fMRI data. ICA assumes independence between components while DL assumes sparseness of the components.

Another class of methods used to analyse resting state fMRI time series is clustering approaches. Clustering is the procedure of dividing a set of unlabelled data into a number of groups (clusters), in such a way that similar in nature samples belong to the same cluster, while dissimilar samples become members of different clusters [4]. The aim of clustering is to maximize the level of similarity between data points by grouping data points into non-overlapping clusters. Therefore, clustering results may be more comparable to traditional functional connectivity results, as they can directly reflect functional connections among brain regions. In [41] a clustering method based on graph theory was proposed. More specifically a connectivity graph was constructed based on correlations between voxels, and then the normalized-cut (spectral clustering) clustering method was used. This method was applied to a group of subjects and the results were found to be consistent with those reported in the literature. In [33] a summarization of original fMRI time series was made by applying an anatomical prior template to the original fMRI data, followed by an hierarchical cluster analysis. The results showed a hierarchical structure of the brain, where at the highest level of the hierarchy six large RSNs were identified. In [13] the well-known k-means clustering algorithm was used to analyse fMRI data. The results revealed the division of human brain into two large systems. An extension of k-means, the fuzzy c-means algorithm, was used to identify resting state networks in [19]. Also, in [43] a comparison of the k-means algorithm with the spectral clustering was presented for discovering the functional connectivity of the brain. Finally, in [31] a regression mixture model was proposed for clustering of resting state fMRI data on a slice-by-slice experimental design.

In this paper we propose a compact framework for discovering RSNs of the brain based on regression mixture modeling and simultaneous multi-stage data processing. It substantially improves and extends our previous work presented in [31]. More specifically, the contribution of our work lies mainly on four aspects:

- We perform a **4D data analysis** where we collect all brain voxels and construct fMRI time series across all slices. Clustering is then applied to all these sequential data and thus the estimated cluster regions have 3D geometrical structure.
- Besides single subject analysis, we perform a group analysis using data from two fMRI datasets.

- The proposed regression mixture model incorporates **efficient functions** as derived by the enforcement of prior distributions on model parameters which act as constraints. These include regularized capabilities through the use of a sparse students't prior over the model regression coefficients, as well as smooth properties via Markov random field (MRF) prior over the voxels' labels.
- We introduce a new **non-parametric prior** for capturing spatial characteristics of fMRI data. This is based on a softmax procedure and provides a simple and low-cost mechanism for estimating the mixing probabilities-labels, which acts as a mean filter on the lattice-based structure of brain.
- Cluster analysis is performed on a regression mixture platform. This has the advantage of creating probabilistic **generative models** for every cluster and therefore for every RSN of brain. Generative models can be seen very powerful in explaining how observed data are generated by the underlying (neuronal) system.

A maximum a posteriori expectation maximization algorithm (MAP-EM) [10], [26] is applied to iteratively estimate the regressions model parameters and fit the input fMRI data. This leads to update rules of all model parameters in closed form during the M-step and improves data fitting. This results into division of data into a number of K clusters and thus the identification of the RSNs of brain. Each cluster is probabilistically described with a regression mechanism (generative model) that can be used for further analysis. We evaluate the performance of the proposed methodology by clustering a set of fMRI time series using a variety of artificial and real data sets. Comparative results demonstrate improvements on the performance and indicate that our method offers both flexibility and robustness obtaining superior modeling solutions. Since the ground truth is already known for all artificial datasets, we have used the percentage of correct classification (purity) and the normalized mutual information (NMI) quantities for evaluating the performance of each method.

The remaining of this paper is organized as follows: In section 2 we present the general framework of the regression mixture model, while in section 3 the proposed probabilistic framework is described along with its spatial and regularized properties. To assess the performance of the proposed methodology we present in section 4 numerical experiments. The experiments are divided into two categories. In the first category, artificial 4-D data sets, that simulated brain's function, are used, while, in the second category of experiments real fMRI time series from two datasets are used to evaluate the proposed method. Finally, in section 5 we provide conclusions and suggestions for future research.

2. fMRI data analysis using probabilistic mixture models

Clustering is an active and challenging research problem with many applications in various scientific fields. For this reason a large number of methodologies have

been used to address this problem. From all these methodologies special attention has attract the probabilistic mixture modeling which is a model-based approach for clustering that offers many advantages, such as a platform to qualitative evaluate the clustering solution [4],[26]. However, the fMRI data are time - series and this property must be taken into account when the clustering procedure is executed. In the case of clustering time series the data have one or both of the following two features: first they are of very large dimension, and thus conventional clustering methods may found difficulties, and second they are not of equal length and thus conventional clustering methods cannot straightforwardly be applied. To avoid the above difficulties, we can assume a parametric model for the data and then perform the clustering based on that model.

In our case, we have followed a 4D analysis by considering fMRI time-series from all slices of the brain. In particular, let $\mathbf{y}_n^{(s)}$ be a sequence of values measured at T successive time instances x_l, i.e. $\mathbf{y}_n^{(s)} = \{y_{nl}^{(s)}\}_{l=1,\cdots,T}$. This corresponds to the n-th position of the s-th slice. Thus, we define the total N fMRI time-series of all S slices as: $\mathbf{Y} = \{\mathbf{y}_1^{(1)}, \mathbf{y}_2^{(1)}, \cdots, \mathbf{y}_{N_1}^{(1)}, \mathbf{y}_1^{(2)}, \mathbf{y}_2^{(2)}, \cdots, \mathbf{y}_{N_2}^{(2)}, ..., \mathbf{y}_1^{(S)}, \mathbf{y}_2^{(S)}, \cdots, \mathbf{y}_{N_S}^{(S)}\}$, where $N = N_1 + N_2 + \cdots + N_S$. The set $\mathbf{Y}$ determines the input to our method and the task is to discover 3D brain regions with the same functionality among all slices' positions.

A compact generative scheme for modeling fMRI time series is the linear regression models described by the next equation:

$$\mathbf{y}_n^{(s)} = \mathbf{X}\mathbf{w}_n^{(s)} + \mathbf{e}_n^{(s)} \ , \tag{1}$$

where $\mathbf{w}_n^{(s)}$ is the vector of the (unknown) linear coefficients. The term $\mathbf{e}_n^{(s)}$ describes the noise and it is assumed to be zero mean Gaussian with variance $\sigma^{2(s)}_n$, i.e. $\mathbf{e}_n^{(s)} \sim \mathcal{N}(0, \sigma^{2(s)}_n \mathbf{I})$. Finally, $\mathbf{X}$ is the design matrix where its choice plays an important role for the data analysis. In the literature, many design matrices have been proposed. For example when polynomial or splines models are used then Vandermonde or B-splines matrices are appropriated. Also, when evidence suggests that the time series can be described well from specific basis functions such as sines or wavelets, then dictionaries based on the Fourier Transform or the Wavelet Transform can be used to construct the design matrix. Finally, another approach is to assume a kernel design matrix using an appropriate kernel basis function over time instances $\{x_l\}_{l=1}^T$. A common choice is to consider Gaussian kernel matrix

$$[X]_{lk} = K(x_l, x_k; \lambda) = \exp\Big(- \frac{(x_l - x_k)^2}{2\lambda} \Big) \ ,$$

where λ is a scalar parameter. In addition, the design matrix may contain information about the experimental paradigm of fMRI experiment [27].

Following the regression function of Eq.(1), the conditional probability density of the fMRI sequence $\mathbf{y}_n^{(s)}$ is also Gaussian

$$p(\mathbf{y}_n^{(s)} | \theta_n^{(s)}) = \mathcal{N}(\mathbf{X}\mathbf{w}_n^{(s)}, \sigma^{2(s)}_n \mathbf{I}) \ ,$$

where $\theta_n^{(s)}$ is the set of model parameters, i.e. $\theta_n^{(s)} = \{\mathbf{w}_n^{(s)}, \sigma^{2(s)}_n\}$.

The motivation behind the mixture models is that the available data may include unobserved groups and by incorporating such structure we could obtain more accurate predictions. The clustering problem is referred to uncover that group structure of data, called clusters. In model-based approaches we assume that each cluster is described by a generative model and the aim of clustering is focused on discovering an optimal set of such models in order to best fit the data. Mixture models provide an efficient and flexible architecture that is suitable for clustering which is used as a data-generating process for the observed data. In particular it is assumed that the data in each group or cluster is generated by a specific distribution and the combined data stems from a convex combination of distributions. Clustering is then done by learning the parameters of these models and the associated probabilities. Through the clustering procedure, each data is then assigned to the mixture component that most likely generated it. The probability density function, describing the data generation process, is given by:

$$f(\mathbf{y}_n^{(s)}|\Theta) = \sum_{j=1}^{K} \pi_j p(\mathbf{y}_n^{(s)}|\theta_j) \ , \tag{2}$$

where π_j are the weights (prior probabilities) of every cluster that satisfy the constraints: $\pi_j \geq 0$ and $\sum_{j=1}^{K} \pi_j = 1$, while Θ is the set of all mixture model parameters, i.e $\Theta = \{\pi_j, \theta_j\}_{j=1}^{K}$.

The task of clustering lies on the estimation of the model parameters that is usually obtained through the maximum likelihood (ML) framework and the Expectation-Maximization (EM) algorithm [10], where the log-likelihood function is:

$$l(\Theta) = \log p(\mathbf{Y}|\Theta) = \sum_{s=1}^{S} \sum_{n=1}^{N_s} \log \Big\{ \sum_{j=1}^{K} \pi_j p(\mathbf{y}_n^{(s)}|\theta_j) \Big\}. \tag{3}$$

Assignment of the data to the K groups is then achieved according to the maximum of the posterior probabilities of component membership:

$$z_{nj}^{(s)} = \frac{\pi_j p(\mathbf{y}_n^{(s)}|\theta_j)}{f(\mathbf{y}_n^{(s)}|\Theta)} \ . \tag{4}$$

$$cluster_n^{(s)} = \arg\max_j \{z_{nj}^{(s)}\} \tag{5}$$

The above ML-based mixture modeling presents two major drawbacks: At first, spatial correlations of data that exist naturally, cannot be taken into account. Secondly, the order of the regression model that is related to the complexity of method, is not automatically determined as it is desired. In next section we describe a compact scheme that incorporates the above issues to the body of classical regression mixture models.

3. Regression mixture analysis with advanced properties

In order to avoid the drawbacks of ML approach, and in addition to weakened the effect of noise in the clustering results, local spatial interactions among neighboring fMRI time series must be taken into account. Spatial interactions can be introduced by using a spatial Gaussian filter. However, this approach makes the assumption that spatial interactions are the same among all time series and this assumption can produce blurred results. This means that spatial properties among a small group of fMRI time-series can be lost or may extended beyond their actual boundaries affecting the time-series outside this group. A more advanced approach to spatial regularization is through the use of Markov Random Field (MRF) prior [12] which models the conditional spatial dependence between fMRI time series.

Due to brain spatial organization, fMRI time series contain spatial interactions between them. The above statement is supported by the fact that adjacent voxels tend to have similar activity. Furthermore, fMRI studies have shown that spatial interactions can be observed among remote brain regions. Spatial interactions can be incorporated into our model through the mixing probabilities. More specifically, we assume that any sequence $\mathbf{y}_n^{(s)}$ has a set of labels $\pi_{nj}^{(s)}$ associated with the degree of belongingness to any cluster j, $j = 1, \ldots, K$. We treat these parameters as random variables that have also the constraints $\pi_{nj}^{(s)} \geq 0$ and $\sum_{j=1}^{K} \pi_{nj}^{(s)} = 1$.

Imposing spatial smoothness is a significant key to certain image processing applications since it is an important a priori known property of images. Examples of such applications include denoising, restoration, inpainting and image segmentation problems [12,21]. In a probabilistic framework, smoothness is expressed through a prior imposed on image features. This is achieved by Markov Random Filelds (MRFs) as inspired by the Ising model, that utilized them as a powerful tool to impose spatial coherence on mixture models and image segmentation. A common method using MRF is to impose spatial smoothness directly on the hidden variable, which indicates the label of image pixels. Due to the coupling of model parameters, Hidden Markov Random Field (HMRF) is not computationally feasible, simulation and variational methods are used to make it tractable, such as mean-field [21]. However the computational cost of these methods remains quite high. Another commonly used spatial mixture model based on MRF is Spatially Variant Mixture Model (SVMM) [6,46] that imposes spatial constraint on the prior probability indicating the label of pixels. More specifically, MRF introduces a prior distribution that takes into account the neighborhood dependency or relationship among the neighboring pixels. Then, the posteriori density function consists of two terms: a likelihood term which is exclusively based on the intensity distribution of the data and captures the pixel intensity information, and a biasing term that uses the MRF component capturing the spatial location information. Thus, through the application of a suitable prior density function a mechanism is introduced that models the local correlation in the parameter estimation process.

A well - known approach to introduce MRFs related to image models is to

define them on a lattice. In an MRF the sites are related to one another via a neighborhood system. It can characterized by a Gibbs distribution according to an energy function which is a sum of clique potentials over all possible cliques of the lattice. A clique is defined as a subset of sites in which every pair of distinct sites are neighbors depending on the local configuration. More specifically, MRF assumes that the data are related to each other via a neighborhood system defined as $\mathcal{N} = \{\mathcal{N}_n, n = 1, \cdots, N\}$, where $\mathcal{N}_n$ is the set of neighboring sites of n. According to the Hammersley-Clifford theorem [21], an MRF can equivalently be characterized by a Gibbs distribution. Thus,

$$P(\mathbf{x}) = \frac{1}{Z} \exp\{-U(\mathbf{x})\} \tag{6}$$

where

$$Z = \sum_{\mathbf{x} \in \mathcal{X}} \exp\{-U(\mathbf{x})\} \tag{7}$$

is a normalizing constant called the partition function, and $U(\mathbf{x})$ is an energy function of the form

$$U(\mathbf{x}) = \sum_{c \in \mathcal{C}} V_c(\mathbf{x}) \tag{8}$$

which is a sum of clique potentials $V_c(\mathbf{x})$ over all possible cliques. For more detail on MRF and Gibbs distribution see [21].

For the standard GMM the degree of belief that the n-th time series of s-th slice belongs to the j-th cluster is express through $z_{nj}^{(s)}$ (Eq. 4). However, in this expression spatial correlations do not exist. This is achieved by inserting an appropriate prior distribution over the mixing probabilities, considering that there is an influence of neighboring positions for estimating the cluster labels of observation $\mathbf{y}_n^{(s)}$. In particular, we consider a Gibbs distribution over mixing labels parameters, that establishes spatial dependencies and offers smoother solutions. We assume a Gibbs potential function of the following formulation:

$$\vartheta_{nj}^{(s)} = \sum_{m \in \mathcal{N}_n^{(s)}} z_{nj}^{(s)} z_{mj}^{(s)} \ . \tag{9}$$

This function acts as a spatially variant smooth filter to the posterior values (estimations) and it works like a voting system i.e. a particular voxel will take the class label of the majority of voxels found in its neighborhood. *It must be noted that we consider as neighborhood $\mathcal{N}_n^{(s)}$ the set containing voxels that are vertically, horizontally and diagonally adjacent to voxel n ($3 \times 3 \times 3$ grid area).*

The quantity $\vartheta_{nj}^{(s)}$ can be seen as a metric that describes our belief that the n-th time series belongs to j-th cluster. This is expressed as a weighted average of $z_{nj}^{(s)}$, using as weights the probabilities of neighborhood $z_{mj}^{(s)}, m \in \mathcal{N}_n^{(s)}$ (see Eq.9). Furthermore, we can observe that the following inequality holds:

$$0 \leq \vartheta_{nj}^{(s)} \leq |\mathcal{N}_n^{(s)}| \ .$$

There are two marginal cases: If $z_{mj}^{(s)} \to 0$, $m \in \mathcal{N}_n^{(s)}$ then $\vartheta_{nj}^{(s)} \to 0$. This happens when there is totally disagreement with the cluster probabilities of neighboring sites. In the second case, $z_{mj}^{(s)} \to 1$ leads to $\vartheta_{nj}^{(s)} \to |\mathcal{N}_n^{(s)}|$. This means that we have perfect agreement between the examined position its neighborhood. Finally, the updated rule for the mixing probabilities $\pi_{nj}^{(s)}$ is given by the *softmax* operation:

$$\pi_{nj}^{(s)} \propto \frac{\exp\left(\vartheta_{nj}^{(s)}\right)}{\sum_{k=1}^{K} \exp\left(\vartheta_{nk}^{(s)}\right)} \tag{10}$$

Note that the above formulation meets the constraints of $\pi_{nj}^{(s)}$ (positivity and summation to one). Another advantages of softmax is its simplicity and its non-parametric nature. The softmax operation is a normalized exponential and it represents a smoothed version of the max function. Also, this operation holds another one useful property with respect to the mixing probabilities. In general, for the derivatives with respect to the mixing coefficients, we need to take account of the constraints (sum to one) which follow from the interpretation of the mixing coefficients as prior probabilities. However, in our case, this can be done easily by expressing the mixing coefficients with the softmax transformation.

When a regression model is used, a serious problem is how to determine its order M, i.e. the number of linear regression coefficients $\mathbf{w}_j$. Accurate estimation of the order is crucial since models of small order may lead to under-fitting, while large values of M may become responsible for data over-fitting. Hence, the clustering performance may be undermined by the improper model order. Reguralization approaches provides a solution to this problem. Among them, the Bayesian regularization framework is the most notable, giving us a elegant solution to this problem [39,4]. Within this framework a large value of order M is assumed. However, a heavy tail prior distribution is used over the regression coefficients. This particular prior put in action a procedure where the most important coefficients are kept while zeroing the remaining coefficients.

To impose sparse properties over the regression coefficients, an hierarchical model, with two - levels of hierarchy, is used[39]. At the first level, we consider a zero-mean Gaussian distribution over the regression coefficients:

$$p(\mathbf{w}_j|\boldsymbol{\alpha}_j) = \mathcal{N}(\mathbf{w}_j|\mathbf{0}, \mathbf{A}_j^{-1}) = \prod_{l=1}^{M} \mathcal{N}(w_{jl}|0, \alpha_{jl}^{-1}) \ , \tag{11}$$

where $\mathbf{A}_j$ is a diagonal matrix containing the M components of the precision (inverse variance) vector $\boldsymbol{\alpha}_j = (a_{j1}, \ldots, a_{jM})$. Then, at a second level, precision can be seen as hyper-parameters that follow a Gamma prior distribution:

$$p(\alpha_j) = \prod_{l=1}^{M} \Gamma(\alpha_{jl}|b, c) \propto \prod_{l=1}^{M} \alpha_{jl}^{b-1} \exp^{-c\alpha_{jl}} \ . \tag{12}$$

Note that both Gamma parameters b and c are a priori set to zero so as to achieve uninformative priors. The above hierarchical prior is a sparse prior, and more specif-

ically is a Student's-t distribution. An important property of this prior is that enforces most of the values α_{jl} to be large and thus eliminating the effect of the corresponding coefficients w_{jl} by setting to zero. As we see, the order M for every cluster is automatically selected and, hence, over-fitting is avoided. Sparsity is a property that has widely been used in fMRI data analysis with great success [11,30,29,28,3].

The clustering procedure becomes now a Maximum-A-Posteriori (MAP) estimation problem, where the MAP log-likelihood function is given by

$$l_{MAP}(\Theta) = \sum_{s=1}^{S}\sum_{n=1}^{N_s}\log\{\sum_{j=1}^{K}\pi_{nj}^{(s)}p(\mathbf{y}_n^{(s)}|\theta_j)\} + \sum_{j=1}^{K}\left\{\log p(\mathbf{w}_j|\boldsymbol{\alpha}_j) + \log p(\boldsymbol{\alpha}_j)\right\}. \tag{13}$$

where $\Theta = \{\theta_j = (\mathbf{w}_j, \boldsymbol{\alpha}_j, \sigma_j^2)\}_{j=1}^{K}$.

Employing the EM algorithm to MAP estimation requires at each iteration the conditional expectation values $z_{nj}^{(s)}$ of the hidden variables to be computed first (E-step):

$$z_{nj}^{(s)} = \frac{\pi_{nj}^{(s)}p(\mathbf{y}_n^{(s)}|\theta_j)}{\sum_{k=1}^{K}\pi_{nk}^{(s)}p(\mathbf{y}_n^{(s)}|\theta_k)}. \tag{14}$$

Also, during the M- step the following updated rules are obtained:

$$\mathbf{w}_j = \Big[\Big(\sum_{s=1}^{S}\sum_{n=1}^{N_s}z_{nj}^{s}\Big)\frac{1}{\sigma_j^2}\mathbf{X}^T\mathbf{X} + \mathbf{A}_j\Big]^{-1} \cdot\frac{1}{\sigma_j^2}\mathbf{X}^T\Big(\sum_{s=1}^{S}\sum_{n=1}^{N_s}z_{nj}^{(s)}\mathbf{y}_n^{(s)}\Big), \tag{15}$$

$$\alpha_{jl} = \frac{1+2c}{w_{jl}^2+2b}, \tag{16}$$

$$\sigma_j^2 = \frac{\sum_{s=1}^{S}\sum_{n=1}^{N_s}z_{nj}^{(s)}\|\mathbf{y}_n^{(s)} - \mathbf{X}\mathbf{w}_j\|^2}{T\sum_{s=1}^{S}\sum_{n=1}^{N}z_{nj}^{(s)}}. \tag{17}$$

The above equations are applied iteratively until convergence. Furthermore, $\pi_{nj}^{(s)}$ are calculated by using Eq. (10). At the end, we assign cluster labels to each sequence $\mathbf{y}_n^{(s)}$ according to the maximum posterior probability (Eq. 14). A schematic representation of the overall data analysis procedure can be seen in Fig. 1. After image acquisition and data preprocessing, the step of statistical analysis is taken place in order to find the RSNs (decision step). In our approach the statistical analysis step includes the estimation of model parameters. After that a simple rule is applied on posterior probabilities z_{nj} to find the clusters, and hence the RSNs.

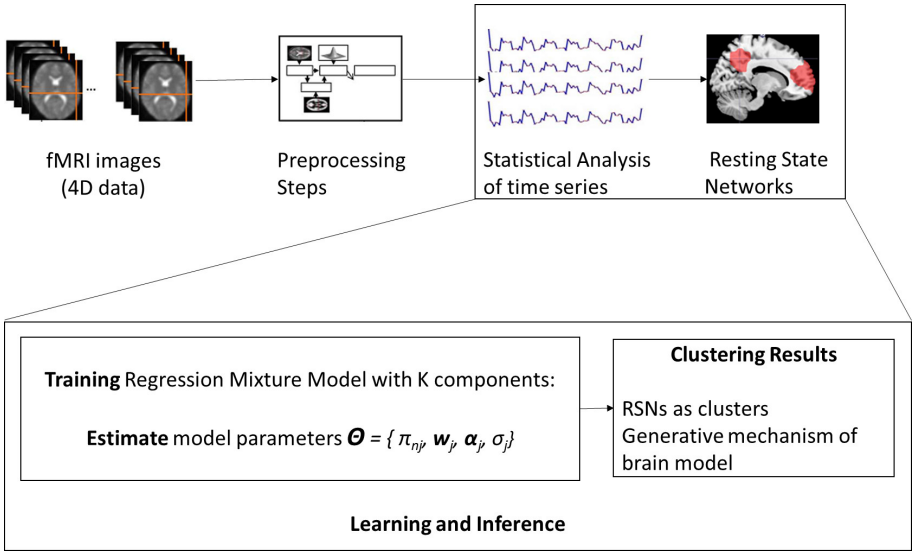

Fig. 1. A four - step schematic representation of the overall procedure for fMRI time series analysis. The proposed iterative algorithm is taking place to the step "Statistical Analysis of time series".

4. Experimental results

The proposed regression mixture model has been evaluated using a variety of artificial datasets and real benchmarks. For initializing the EM algorithm we have executed 100 two-EM-steps runs with random initialization and keep the best one according to the log-likelihood function. After that the EM is normally executed until convergence. In the simulation data the number of components equals to the preselected signal sources. In the human data, we visually compared the results with the standard resting state networks of the normal brain after multiple trials with different number of components.

This section is organized as follows: first, we present the experiments with simulated data. Also, at this stage of experiments, a comparison with various clustering algorithms is performed. Then, we present experiments using two real resting - state fMRI datasets. In the case of real datasets, our method was also compared with the temporally concatenated ICA approach using the FSL Melodic ICA toolkit [a].

4.1. *Experiments with simulated data*

The purpose of making experiments with simulated dataset is to examine the capability of our method to detecting and differentiating the true sources of signals and their spatial profile. During the experiments with simulated fMRI data, we have

[a]https://fsl.fmrib.ox.ac.uk/fsl/fslwiki/MELODIC

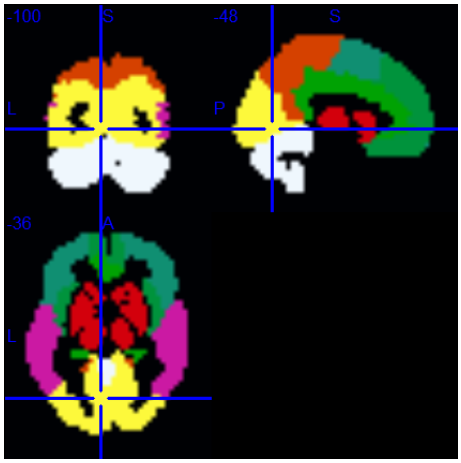

Fig. 2. Axial, Coronal and Saggital view of 8 clusters

created 4-D datasets of time series using linear regression models with known design matrix and regression coefficients. To create the spatial patterns in 3D space, we build a 3D brain model by using the Automated Anatomical Labeling (AAL) digital brain atlas. The spatial patterns are constructed by merging various brain regions from above atlas. A graphical representation of them is provided in Fig. 2. In the experiments with simulated data the number of clusters was set to 8 (K=8). and for each SNR level we execute 50 Monte Carlo simulations. Finally, we compared the proposed method with:

- the classical k - *means* algorithm
- the *rGMM_ML* method. This a simplified model of our proposed method without using spatial and sparse properties. This method is described in section 2.
- the classical *GMM_ML* method with a diagonal covariance[4].

Since we are aware of the ground truth, the quality of each clustering approach was measured using two evaluation criteria:

- the classification accuracy, calculated as the percentage of correctly labelled time series, and
- the normalized mutual information (NMI), which is an information theoretic measure based on the mutual information between of the true labelling (Ω) and the clustering ($\mathcal{C}$) normalized by their entropies:

$$NMI(\Omega, \mathcal{C}) = \frac{I(\Omega, \mathcal{C})}{(H(\Omega) + H(\mathcal{C}))/2} \ , \tag{18}$$

where

$$I(\Omega, \mathcal{C}) = \sum_k \sum_j P(\omega_k, c_j) \log \frac{P(\omega_k, c_j)}{P(\omega_k)P(c_j)} \ ,$$

$$H(\Omega) = -\sum_k P(\omega_k) \log P(\omega_k) \ , \ H(\mathcal{C}) = -\sum_k P(c_k) \log P(c_k) \ .$$

The quantities $P(\omega_k)$, $P(c_j)$ and $P(\omega_k, c_j)$ are the probabilities of a sequence being in class ω_k, cluster c_j and in their intersection, respectively, and are computed based on set cardinalities (frequencies).

4.1.1. *Experiments with Gaussian time series*

In the first series of experiments we have created time series according to a known regression model, i.e. known design matrix and regression coefficients. In particular, we have used a discrete cosine transform (DCT) matrix of size NxN, where N the length of time series (in our case $N = 128$). In these time series, we have added white Gaussian noise of various SNR levels. To conclude, each time series $\mathbf{y}$ is created by linear regression model where the design matrix, the regression coefficients and the Gaussian distribution of noise is known i.e. $\mathbf{y} = \mathbf{Xb} + \mathbf{e}$. The product $\mathbf{Xb}$ represents the mean of the cluster. The results, with respect to the aforementioned performance measures, are shown in Fig. 3 in terms of errorbars. We can observed that the proposed method clearly outperforms all other approaches in terms of accuracy and NMI. Also, by examining the performance of the proposed method, the GMM_ML and the rGMM_ML we can see the usefulness of adopting a regression model for modeling the time - series. The classical GMM_ML method presents the worst performance over all mixture based methods. This is expected since the regression based mixtures model more accurately the structures that can be found inside a time series such as temporal correlations. Overall, the constraints, that are imposed by the regression model, to the mean and the covariance of each mixture's component provide us with more accurate modeling of the time series, which is reflected into better performance.

4.1.2. *Experiments with non-Gaussian time series*

In the non Gaussian case we have followed the same strategy as previous. The only difference is that the mean of each cluster is transform by *sinh* function, i.e. $\mathbf{y} = sinh(\mathbf{Xb}) + \mathbf{e}$. The results are shown in Fig. 3 in terms of errorbars. We can observe that the proposed method presents, clearly, outperforms, in terms of accuracy and NMI, all other methods in the case of 10,5,0,-5 dB SNR, while in the case of -10dB SNR, the proposed method and the k-means present similar performance. Finally, we can see that the performance of each method is degraded when non Gaussian time series are used. It is worth to point here that in very noisy environments (below -5 dB) we observed a significant deterioration in the

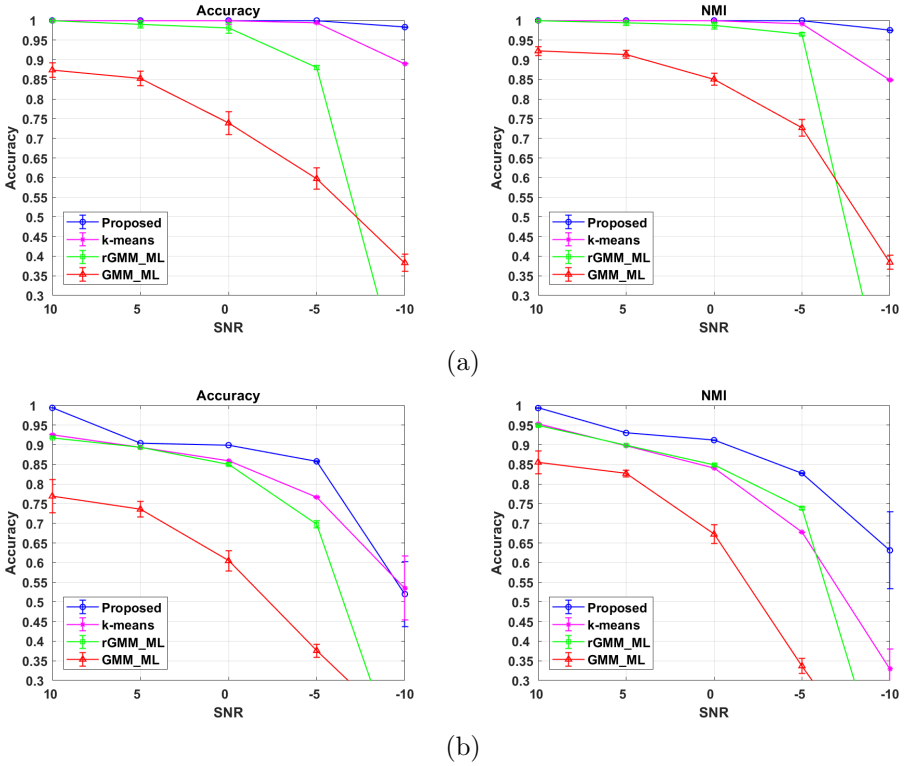

Fig. 3. Results on simulated datasets (a) Gaussian time series and (b) non-Gaussian time series.

performance of rGMM_ML method. This is expected since this method is based on ML principle and it is overfitted in the noisy data. Concluding this section, we can observed that a regression based mixture model with spatial properties is very useful in cases where spatial correlation between the time series are expected.

4.2. *Experiments using real fMRI time series*

Our experiments in the previous section have shown that the proposed Gaussian Mixture model presents much better performance from many variants of mixture modelling idea so in this section we use only our method from mixture modelling approaches. We provide comparisons of our method with the k-means and the ICA approach. The k-means method is used as an alternative clustering approach and it can be considered as the baseline method for any clustering procedure. The comparison with the ICA approach is based on the fact that this method is widely used for the identification of brain networks in resting state fMRI data. In the first series of experiments we perform single subject analysis and group analysis by using our method and the k-means. Also, a qualitative comparison between the two methods

is performed. These series of experiments have the goal to check if our method produces brain networks consistent with those reported in the literature. Then, in the second series of experiments, a more thorough quantitative and qualitative comparison of our method with the ICA approach is performed. In addition to the above, we examine the behaviour of our method across different fMRI datasets.

Experiments were made using real fMRI data. We downloaded two resting - state fMRI datasets from the '1000 Functional Connectomes' Project. The name of the first dataset (Dataset1) is 'Berlin_Margulies'[b]. This dataset contains resting state fMRI data from 26 healthy subjects, where we have used the first ten subjects for performing our study. Also, we have downloaded the Neurocon[c] dataset[1] (Dataset2) from '1000 Functional Connectomes' Project. This dataset contains resting state fMRI data from 27 PD patients and 16 age-matched normal controls. For the resting-state scan, subjects were instructed to close their eyes and think nothing in particular without falling asleep. In order to perform our analysis we selected the first 3 subjects belonging to the control group.

Before analyzing the fMRI data, several standard preprocessing steps were made using the SPM package [d]. These include: realignment, co-registration, segmentation, normalization and spatial smoothing. After that, a mask, based on Harvard Oxford Atlas, was applied in order to exclude regions that do not contain activation. Furthermore, the time series have been filtered to keep the frequency contents from 0.001Hz to 0.09Hz. In addition, when we perform a group analysis the time series of subjects have been concatenated into one large dataset. Also, in group analysis case, each time series has been downsampled by a factor of 4 in order to reduce the size of the data. A downsampling factor below this value will affect the low frequency components related to resting state time series. Finally, the number of clusters was set to be $K = 7$. This number has been selected after applying our algorithm many times with different number of clusters and compared the results with well - known resting state networks.

4.2.1. *Single Subject analysis*

At first, we perform a single subject analysis by using fMRI data of the first two subjects from Dataset1. RSNs for the first subject using our method and the k-means algorithm are shown in Figs 4 and 5, respectively. While the RSNs for the second subject using our method and the k-means algorithm are shown in Figs 6, 7, respectively.

The obtained clusters of our method for subject 1 are shown in Fig. 4. More specifically, we can observe that cluster 1 contains the middle temporal gyrus (BA 21), the temporopolar area (BA 38), the superior temporal gyrus (BA 22) and the

[b]http://fcon_1000.projects.nitrc.org/fcpClassic/FcpTable.html
[c]http://fcon_1000.projects.nitrc.org/indi/retro/parkinsons.html
[d]SPM web page http://www.fil.ion.ucl.ac.uk/spm

Pars triangularis (BA 45). It can be recognized as a frontal temporal network. Cluster 2 contains the Primary Motor Cortex (BA 4), the Supplementary Motor Area (BA 6), the Primary Somatosensory Cortex (BA 1,2 and 3), the Somatosensory Association Cortex (BA 5) and the Frontal Eye fields (BA 8). It is a sensorimotor network. Cluster 3 contains the anterior/dorsolateral prefrontal cortex (BA9/10), parts of cingulate cortex (BA 23/26), and the precuneus (BA 7). It can be recognized as the DMN. Cluster 4 contains the auditory cortex (BA 42) and the superior temporal gyrus. This network is an auditory network. Cluster 5 contains the cingulate cortex (BA 24 and 29), parts of the frontal lobe (BA 46,BA 44, BA 8 and BA 9), and parts of the Somatosensory Association Cortex (BA 7) . It is a salience processing network. Cluster 6 can be recognized as the Visual network. Cluster 7 contains parts of the orbitofrontal area and the inferior temporal gyrus. It is a frontal-temporal network.

The obtained clusters of kmeans algorithm for subject 1 are shown in Fig. 5. Cluster 1 can be recognized as the visual network. Cluster 2 contains parts of frontal lobe (BA 8, 9 44,45 and 46) and parts of Somatosensory Association Cortex (BA 7 and 5). It is an executive processing network. Cluster 3 contains the Inferior temporal gyrus (BA 20), the orbitofrontal area (BA 11), the Pars orbitalis (BA 47), the temporopolar area (BA 38) and the middle temporal gyrus (BA 21). It is a frontal temporal network. Cluster 4 contains the auditory cortex (BA 42) and the superior temporal gyrus (BA 22). It is an auditory network. Cluster 5 contains the Primary Motor Cortex (BA 4), the Supplementary motor area (BA 6), the Somatosensory Association Cortex (BA 5) and the Primary Somatosensory Cortex (BA 1,2 and 3). It is a sensorimotor network. Cluster 6 contains parts of prefrontal cortex (BA 9 and10), parts of cingulate cortex (BA 32 and 23) and the Precuneus (BA 5 and 7). It can be recognized as the DMN. Cluster 7 contains parts of cingulate cortex (BA 29,24 and 23), parts of auditory cortex (BA 41), and parts of the prefrontal cortex (BA 9 and 46). It is a salience processing network.

The obtained clusters of our method for subject 2 are shown in Fig. 6. We see that cluster 1 contains the inferior temporal gyrus (BA 20), the middle temporal gyrus (BA 21), the temporopolar area (BA 38) and the orbitofrontal area (BA 11). It is a frontal - temporal network. Cluster 2 contains parts from Motor Cortex (BA 1,2,3,4 and 5) and parts from Primary Visual Cortex (BA 17). It is a Visual - Motor network. Cluster 3 contains the Precuneus (BA 7), the Anterior prefrontal cortex (BA 10) and parts of cingulate cortex (BA 32 and 23). It can be recognized as the DMN. Cluster 4 contains the Associative visual cortex, the secondary visual cortex and the remaining parts of primary visual cortex (BA 17). It can be recognized as the Visual Network. Cluster 5 contains parts of Cingulate cortex (BA 23, 24 29) and the Somatosensory Association Cortex (BA 7). It is a salience processing network. Cluster 6 contains Brocas area (BA 44), parts of Auditory Cortex (BA 42), parts of Supplementary Motor Areas (BA 6) and parts of frontal lobe (BA 8 - Includes Frontal eye fields). It is a motor - auditory network. Cluster 7 contains

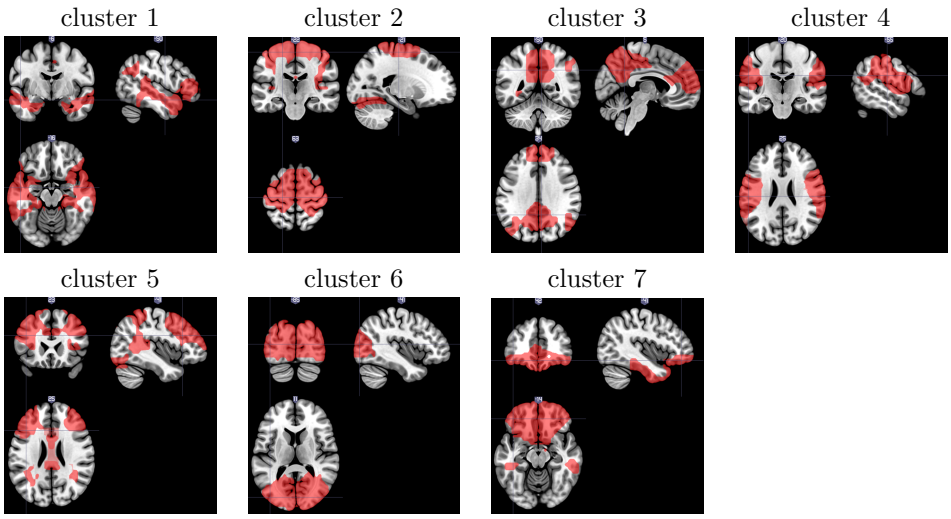

Fig. 4. Subject 1: Axial, Coronal and Saggital view of clusters using our method. Each cluster has been superimposed into the ch256 template of mricrogl toolbox. The red color defines the region of the cluster.

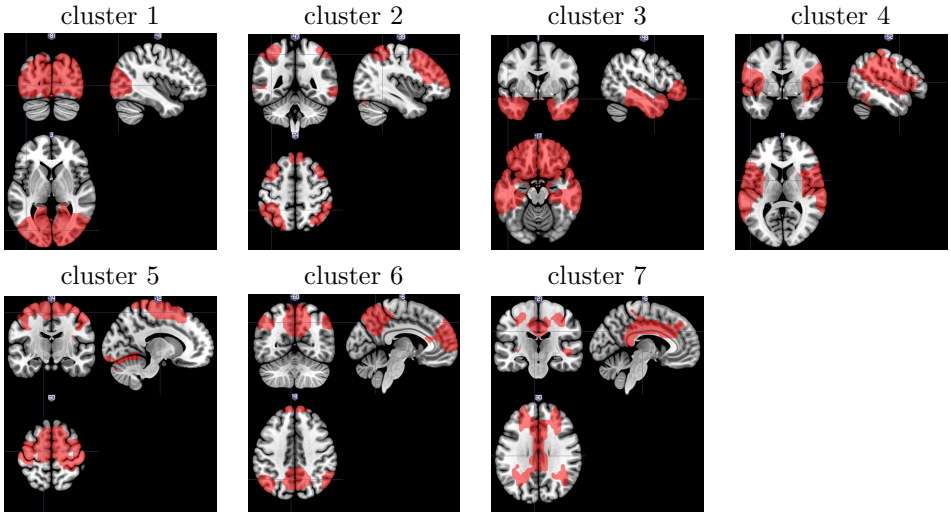

Fig. 5. Subject 1: Axial, Coronal and Saggital view of clusters using kmeans. Each cluster has been superimposed into the ch256 template of mricrogl toolbox. The red color defines the region of the cluster.

parts of inferior frontal gyrus (BA 47), parts of superior temporal gyrus (BA 22), parts of auditory cortex (BA 42) and Brocas area (BA 45). It is frontal-temporal

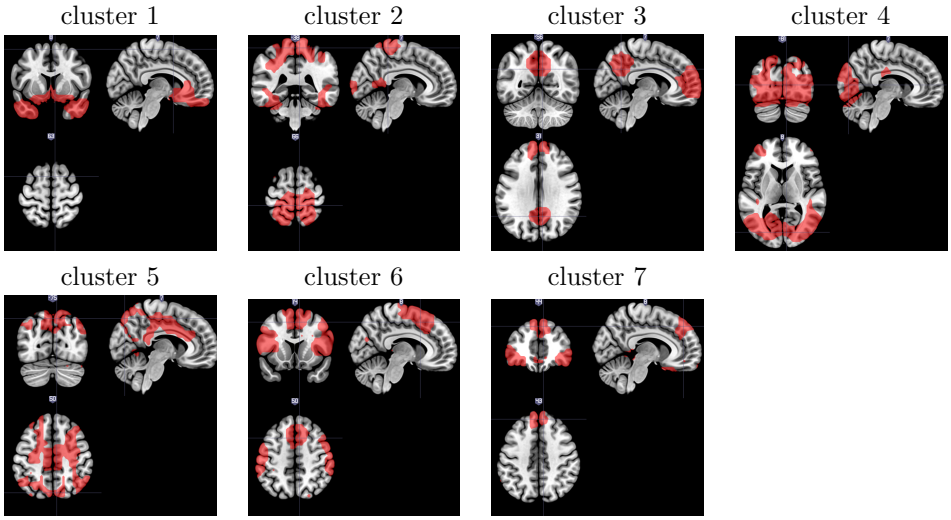

Fig. 6. Subject 2: Axial, Coronal and Saggital view of clusters using our method. Each cluster has been superimposed into the ch256 template of mricrogl toolbox. The red color defines the region of the cluster.

network.

In addition in Fig. 7 the clusters of k-means algorithm are presented for the second subject. Cluster 1 contains the inferior temporal gyrus (BA 20), the middle temporal gyrus (BA 21) and the orbitofrontal area (BA 11). It is a frontal - temporal network, similar to cluster 1 of our method. Cluster 2 contains the Associative visual cortex (BA 19), the Secondary visual cortex (BA 18) and the Primary visual cortex (BA 17). It can be recognized as the Visual Network. Cluster 3 contains the Precuneus (BA5 and 7), the Anterior/Dorsolateral prefrontal cortex (BA 9 and 10) and parts of cingulate cortex (BA 23 and 32). It can be recognized as the DMN. Cluster 4 contains Pars triangularis (BA 45 parts of Broca Areas), Pars orbitalis (BA 47), frontal eye fields (BA 8) and superior temporal gurys (BA 22). It is a frontal - temporal network. Cluster 5 contains the auditory cortex (BA 41), the dorsolateral prefrontal cortex (BA 46) and parts of cingulate cortex (BA 23 and 24). Cluster 6 contains parts of Motor Cortex (BA 5, 1,2,3 and 6) and a part of the Primary Visual Cortex (BA 17). It is a visual-motor network. Cluster 7 contains parts of Primary Somatosensory Cortex (BA 1, 2), pars opercularis (BA 44), and the auditory cortex (BA 42). It is a motor - auditory network.

4.2.2. *Group analysis*

Furthermore to show the effectiveness of our method we perform a group analysis by using the fMRI data of 10 subjects from Dataset1. The provided RSNs by our method are depicted in Fig. 8. By observing the clusters, we can recognized well

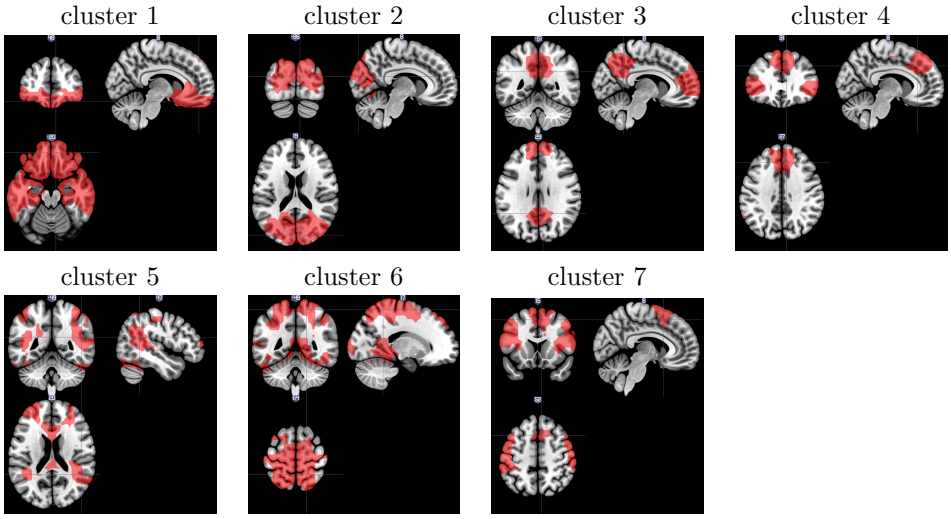

Fig. 7. Subject 2: Axial, Coronal and Saggital view of clusters using kmeans. Each cluster has been superimposed into the ch256 template of mricrogl toolbox. The red color defines the region of the cluster.

known resting state networks such as the Default Mode Network, the visual network and salience network. Cluster 1 contains the Primary Somatosensory Cortex, the Primary Motor Cortex, the Premotor Cortex and the Supplementary Motor Area (SMA), the Primary Auditory Cortex and the superior temporal gyrus. It is a joint network of well-known Sensorimotor and Auditory networks. Cluster 2 contains the dorsolateral/anterior prefrontal cortex and the Precuneus and it can be recognized as the Default Mode Network (DMN). Cluster 3 contains the Primary Visual Cortex and the extrastriate cortex. It can be recognized as the Visual Network. Cluster 4 contains the Brocas Area, the Supramarginal gyrus and parts of the dorsolateral prefrontal cortex (Language processing network). Cluster 5 contains the secondary somatosensory cortex. Cluster 6 contains the orbitofrontal cortex, the entorhinal cortex (part of medial temporal lobe), pars orbitalis (part of inferior frontal cortex), the temporopolar area, the inferior and the middle temporal area and the ventromedial prefrontal cortex. It is a Frontal Temporal network. Cluster 7 contains the anterior cingulate cortex, the posterior cingulate cortex and parts of frontal cortex and it can be recognized as the Salience Network [42].

Similar observations can be obtained by examining the clustering results of k-means algorithm (Fig. 9). More specifically, cluster 1 contains parts of frontal area partially belonging to executive attention network, cluster 2 contains parts of the inferior occipital lobe (parts of extrastriate cortex), of the superior parietal lobe and the occipitotemporal area 37, cluster 3 can be recognized as the Default Mode Network (DMN), cluster 4 is a Fronto temporal Network, cluster 5 is the

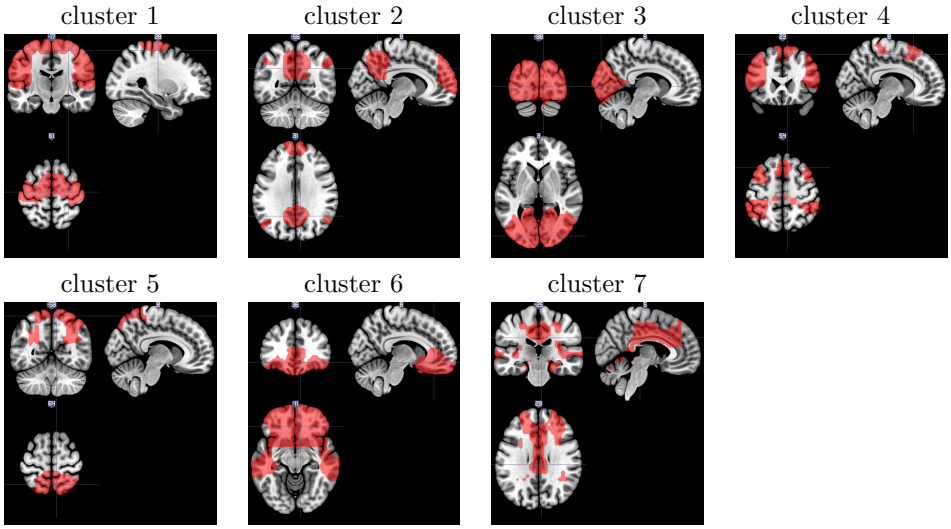

Fig. 8. Group Analysis : Axial, Coronal and Saggital view of clusters using our method. Each cluster has been superimposed into the ch256 template of mricrogl toolbox. The red color defines the region of the cluster/Zmap.

Salience network, cluster 6 can be recognized as Visual network, cluster 7 is the joint network of sensorimotor and auditory networks. We can observe a similarity on the results between our method and the kmeans algorithm, however, a more careful examination reveals differences between two methods. For example, with respect to DMN network we can see that our method includes only the Precuneus, while the kmeans algorithm includes additionally parts of the secondary somatosensory cortex.

4.2.3. *Comparison with Melodic ICA*

In this section we provide a comparison of our approach with the temporally concatenated group ICA using the FSL Melodic ICA toolkit. We applied Melodic ICA in our fMRI data where we set the model order for Melodic ICA to 20, which is a reasonable value based on the findings reported in the literature[36,14]. To perform the comparison, two templates for DMN are used. The first template (DMN1) is provided by GIFT toolbox[e] and the other template (DMN2) is reported in [36f]. The two templates are shown in Fig. 10. In order to detect the DMN using Melodic ICA, we visually examine the 20 components and we choose the functional network which is more similar to DMN templates. We show this network in Fig. 10.

[e]http://mialab.mrn.org/software/gift/
[f]http://www.fmrib.ox.ac.uk/datasets/brainmap+rsns/

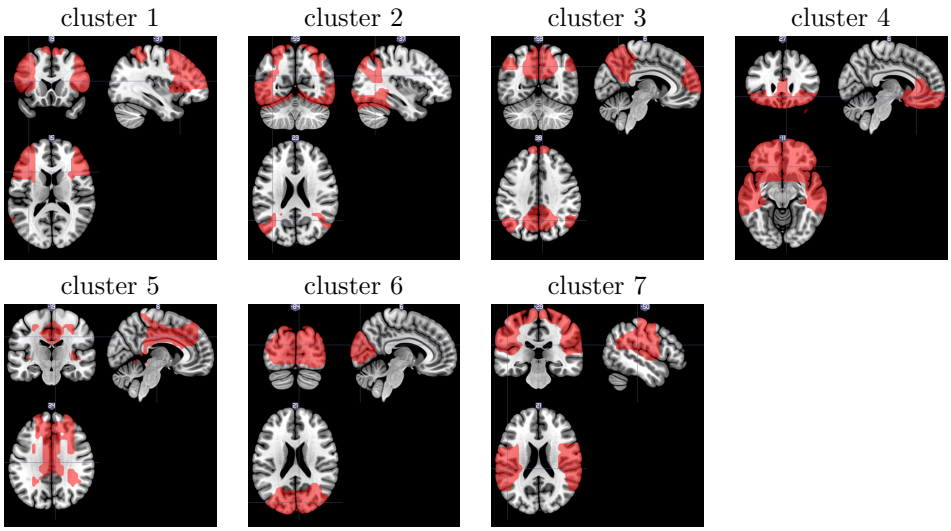

Fig. 9. Group Analysis : Axial, Coronal and Saggital view of clusters using kmeans algorithm method. Each cluster has been superimposed into the ch256 template of mricrogl toolbox. The red color defines the region of the cluster.

To compare the two methods, we follow a similar approach such as these of [23,14]. More specifically, we measure the similarity of corresponding spatial maps provided by the two methods. with the DMN templates. The similarity is obtained by using two measures, the NMI and the Jaccard similarity index [38]. The Jaccard similarity index measures similarity between finite sample sets, and is defined as the size of the intersection divided by the size of the union of the sample sets. In our analysis, the sample sets are the spatial map (cluster) and the DMN template, hence Jaccard similarity index is given by:

$$J(S, D) = \frac{|S \cap D|}{|S \cup D|} \tag{19}$$

where S and D represent the spatial map and the DMN template, respectively. In our analysis we choose for comparison the DMN functional network since it is the most widely studied RSN in the resting-state fMRI literature. Also, from the well - known functional networks, DMN is more consistent and reproducible among various studies. Furthermore, DMN activity helps us to better understand mental disorders such as Alzheimers disease[1]. In Table 1, we provide the results of our analysis. We can observe that our method provides higher values for both measures and both DMN templates, compared to the MELODIC ICA. This is a clear indication that our method can more consistently and reliably identify DMN compared with the commonly-used ICA approach.

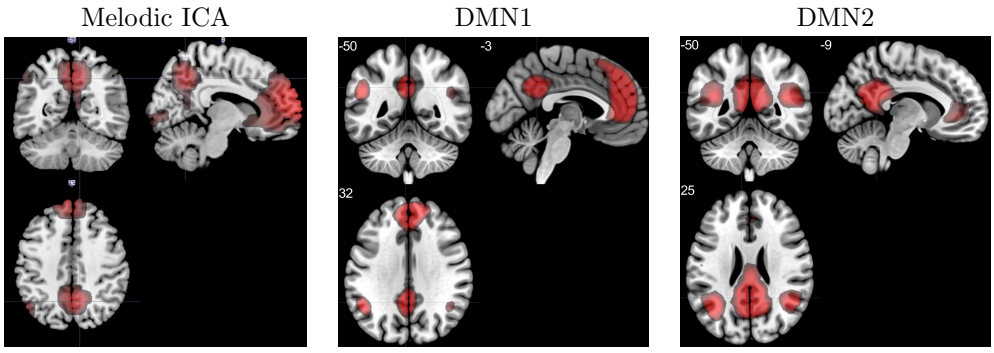

Fig. 10. The DMN using Melodic ICA on Dataset1 and the two DMN templates, DMN1 and DMN2.

Table 1. Similarity Measures

	DMN1		DMN2	
	NMI	Jaccard	NMI	Jaccard
MELODIC ICA	0.3338	0.3477	0.1094	0.1667
GMM	0.3779	0.4032	0.1620	0.1959

4.2.4. *Reproducibility across different datasets*

To evaluate the reproducibility and robustness of our method we use the Dataset2. The goal of this experiment is to show that our method produces brain networks that are consistent across different subjects and datasets. At first we evaluate the obtained clusters by visual inspection (see Fig. 11). We can, visually, observe that clusters 1,2,3,4,5,6 and 7 of dataset1 (see Fig. 8) are similar to clusters 7,3,1,4,5,6 and 2 of dataset2 (see Fig. 11), respectively. In order to provide a quantitative analysis we have also calculate the spatial similarity between the clusters of the two datasets. Spatial similarity maps are provided in terms of Hinton diagrams in Fig. 12. Hinton diagrams are useful in visualizing the values of a 2D array (e.g. a similarity matrix). More specifically, positive and negative values are represented by white and black squares, respectively, and the size of each square represents the magnitude of each value. Spatial similarity between the various clusters is calculated by using the NMI measure and the Jaccard similarity index. According to the results of Fig. 12 we can observe that the clusters 2,3,4,5,6 and 7 from the first dataset are more similar to the clusters 3,1,4,5,6 and 2 of the second dataset, respectively. However, it is worth to point out the behavior of cluster 1 from the first dataset. We can observe that this cluster is very similar with cluster 4 and 7 of the second dataset (with cluster 7 to present a slightly larger value of similarity). Cluster 1 of the first dataset contains regions from the motor and temporal areas

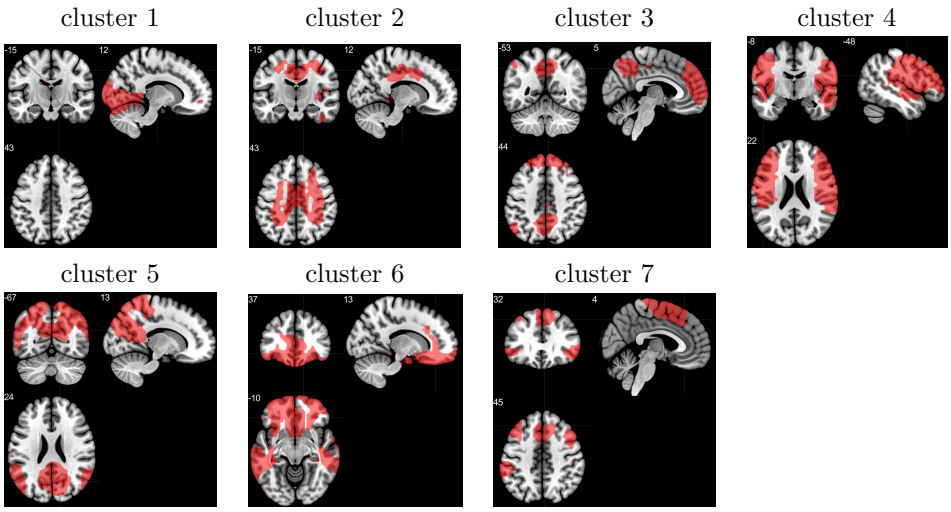

Fig. 11. Group Analysis - dataset2 - gmm : Axial, Coronal and Saggital view of clusters using our method. Each cluster has been superimposed into the ch256 template of mricrogl toolbox. The red color defines the region of the cluster.

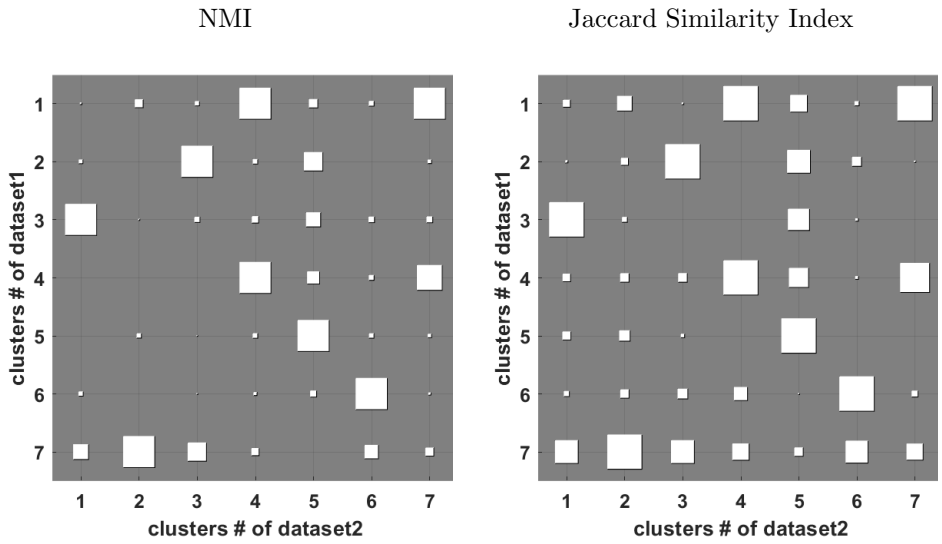

Fig. 12. Hinton Diagrams

of the brain, while cluster 4 of the second dataset contains regions from temporal areas of the brain and cluster 7 of the second dataset contains regions from motor areas. In order to be able a method to reproduce the brain networks across differ-

ent datasets, the Hinton diagrams must have a specific pattern. More specifically, it must be looked as a permutation matrix (i.e. the position of maximum value at each row must be coincided with the position of maximum value at the corresponding column). This pattern can be observe in the reported Hinton diagrams. For example, cluster 3 of Dataset1 is more similar to cluster 1 of Dataset2, also, cluster 1 of Dataset2 is more similar to cluster 3 of Dataset1. The above numerical results are in agreement with those of visual inspection analysis. Concluding this section, the reported results indicating that our method is able to reproduce the reported brain networks, considering the many differences (different subjects, machines and imaging configurations) among the two datasets.

5. Conclusions

In this work a new regression mixture model was proposed for resting state network activity estimation. More specifically, an MRF-based 3-D spatial prior has been introduced over the class labels variables of the mixture model which offers a smooth construction of clusters. Also, a sparse prior is set over the parameters of each cluster regression model that allows the automatic determination of their order. Learning of the model is achieved through the MAP-EM framework that provides an iterative optimization algorithm. Experiments have been made in real resting state fMRI time series and simulated cases with known ground truth. More specifically, we have used our method for single subject analysis as well as for group analysis. The proposed RSNs are consisted with those presented in the literature. A significant benefit of the proposed method is that it enables the construction of generative models due to its nature. Our method is able to provide a mechanism for (re)producing various RSNs of the brain. This can be very useful tool for various applications related to brain modeling and fMRI data analysis.

In the future, we intend to study alternative regression mixture modelling schemes with the incorporation of various properties that we have been encountered in fMRI data. More specifically, a possibility is to study the concept of mixture model order, i.e. estimating the proper number of clusters. This can be seen very useful in many cases, since it can give us new insights into brain's function. Finally, an alternative and more advanced 3D spatial prior, which will incorporated brain topology, could be used over mixing proportions reflecting the structure of the brain.

References

1. L. Badea, M. Onu, T. Wu, A. Roceanu and O. Bajenaru, Exploring the reproducibility of functional connectivity alterations in parkinsons disease, *PLOS ONE* **12** (11 2017) 1–21.
2. C. F. Beckmann, M. DeLuca, J. T. Devlin and S. M. Smith, Investigations into resting-state connectivity using independent component analysis, *Philosophical Transactions of the Royal Society B: Biological Sciences* **360**(1457) (2005) 1001–1013.

3. E. Belilovsky, K. Gkirtzou, M. Misyrlis, A. B. Konova, J. Honorio, N. Alia-Klein, R. Z. Goldstein, D. Samaras and M. B. Blaschko, Predictive sparse modeling of fmri data for improved classification, regression, and visualization using the k-support norm, *Computerized Medical Imaging and Graphics* **46** (2015) 40 – 46.
4. C. M. Bishop, *Pattern Recognition and Machine Learning* (Springer, 2006).
5. B. Biswal, F. Z. Yetkin, V. M. Haughton and J. S. Hyde, Functional connectivity in the motor cortex of resting human brain using echo-planar mri, *Magn. Reson. Med.* **34** (1995) p. 537?541.
6. K. Blekas, A. Likas, N. P. Galatsanos and I. E. Lagaris, A Spatially-Constrained Mixture Model for Image Segmentation, *IEEE Transactions on Neural Networks* **16** (2005) 494–498.
7. J. Cao and K. Worsley, The geometry of correlation fields with an application to functional connectivity of the brain, *The Annals of Applied Probability* **9**(4) (1999) 1021–1057.
8. D. M. Cole, S. M. Smith and C. F. Beckmann, Advances and pitfalls in the analysis and interpretation of resting-state fmri data, *Frontiers in Systems Neuroscience* **4**(8) (2010).
9. J. Damoiseaux, S. A. R. B. Rombouts, F. Barkhof, P. Scheltens, C. J. Stam, S. M. Smith and C. F. Beckmann, Consistent resting-state networks across healthy subjects., *Proceedings of the National Academy of Sciences of the United States of America* **103**(37) (2006) 13848–13853.
10. A. Dempster, L. A. and R. D., Maximum likelihood from incomplete data via the EM algorithm, *Journal of Royal Statistical Society, Series B* **39** (1977) 1–38.
11. G. Flandin and W. Penny, Bayesian fMRI data analysis with sparse spatial basis function priors, *NeuroImage* **34** (2007) 1108–1125.
12. S. Geman and D. Geman, Stochastic relaxation, Gibbs distributions, and the Bayesian restoration of images, *IEEE Trans. on Pattern Analysis and Machine Intelligence* **6** (1984) 721–741.
13. Y. Golland, P. Golland, S. Bentin and R. Malach, Data-driven clustering reveals a fundamental subdivision of the human cortex into two global systems, *Neuropsychologia* **46** (2008) 540?–553.
14. J. Gong, X. Liu, T. Liu, J. Zhou, G. Sun and J. Tian, Dual temporal and spatial sparse representation for inferring group-wise brain networks from resting-state fmri dataset, *IEEE Transactions on Biomedical Engineering* **65** (May 2018) 1035–1048.
15. M. D. Greicius, B. Krasnow, A. L. Reiss and V. Menon, Functional connectivity in the resting brain: A network analysis of the default mode hypothesis, *PNAS* **100**(1) (2003) 253–258.
16. M. D. Greicius, G. Srivastava, A. L. Reiss and V. Menon, Default-mode network activity distinguishes Alzheimer?s disease from healthy aging: Evidence from functional MRI, *PNAS* **101**(13) (2004) 4637–4642.
17. M. J. Jafri, G. D. Pearlson, M. Stevens and V. CalhounVD, A method for functional network connectivity among spatially independent resting-state components in schizophrenia, *Neuroimage* **39** (208) 1666–1681.
18. V. Kiviniemi, J.-H. K. anf J. Jauhiainen, A. Hyvarinen and O. Tervonena, Independent component analysis of nondeterministic fMRI signal sources, *Neuroimage* **19** (2003) 253–260.
19. M. H. Lee, C. D. Hacker, A. Z. Snyder, M. Corbetta, D. Zhang, E. C. Leuthardt and J. S. Shimony, Clustering of Resting State Networks, *PLoS ONE* **7** (2012) p. e40370.
20. K. Li, L. Guo, J. Nie, G. Li and T. Liu, Review of methods for functional brain connectivity detection using fmri, *Computerized Medical Imaging and Graphics* **33**(2)

(2009) 131 – 139.
21. S. Z. Li, *Markov Random Field Modeling in Image Analysis* (Springer Publishing Company, Incorporated, 2009).
22. Y. Liu, K. Wang, C. Yu, Y. He, Y. Zhou, M. Liang, L. Wang and T. Jiang, Regional homogeneity, functional connectivity and imaging markers of Alzheimer's disease: a review of resting-state fMRI studies., *Neuropsychologia* **46**(6) (2008) 1648–1656.
23. J. Lv, X. Jiang, X. Li, D. Zhu, H. Chen, T. Zhang, S. Zhang, X. Hu, J. Han, H. Huang, J. Zhang, L. Guo and T. Liu, Sparse representation of whole-brain fmri signals for identification of functional networks, *Medical Image Analysis* **20**(1) (2015) 112 – 134.
24. D. S. Margulies, J. B?ttger, X. Long, Y. Lv, C. Kelly, A. Sch?fer, D. Goldhahn, A. Abbushi, M. P. Milham, G. Lohmann and A. Villringer, Resting developments: a review of fmri post-processing methodologies for spontaneous brain activity, *Magnetic Resonance Materials in Physics, Biology and Medicine* **23**(5-6) (2010) 289–307.
25. M. J. Mckeown, S. Makeig, G. G. Brown, T. P. Jung, S. S. Kindermann, A. J. Bell and T. J. Sejnowski, Analysis of fMRI data by blind separation into independent spatial components, *Human Brain Mapping* **6**(3) (1998) 160–188.
26. G. McLachlan and D. Peel, *Finite Mixture Models* (New York: John Wiley & Sons, Inc., 2000).
27. V. P. Oikonomou and K. Blekas, An Adaptive Regression Mixture Model for fMRI Cluster Analysis, *IEEE Trans. Med. Imaging* **32** (2013) 649–659.
28. V. P. Oikonomou, K. Blekas and L. Astrakas, A sparse and spatially constrained generative regression model for fmri data analysis, *IEEE Transactions on Biomedical Engineering* **59** (Jan 2012) 58–67.
29. V. Oikonomou, , E. Tripoliti and D. Fotiadis, Bayesian Methods for fMRI Time-Series Analysis Using a Nonstationary Model for the Noise, *IEEE Transactions on Information Technology in Biomedicine* **14** (May 2010 2010) 664–674.
30. V. Oikonomou and K. Blekas, A Sparse Spatial Linear Regression Model for fMRI Data Analysis, in *SETN 2010* (2010) pp. 203–213.
31. V. Oikonomou, K. Blekas and L. Astrakas, Resting state fmri analysis using a spatial regression mixture model, in *Bioinformatics and Bioengineering (BIBE), 2013 IEEE 13th International Conference on* (Nov 2013) pp. 1–4.
32. A. Riaz, M. Asad, E. Alonso and G. Slabaugh, Fusion of fmri and non-imaging data for adhd classification, *Computerized Medical Imaging and Graphics* **65** (2018) 115 – 128.
33. R. Salvador, J. Suckling, M. R. Coleman, J. D. Pickard, D. Menon and E. Bullmore, Neurophysiological Architecture of Functional Magnetic Resonance Images of Human Brain, *Cerebral Cortex* **15**(9) (2005) 1332–1342.
34. Z. Shehzad, A. M. C. Kelly, P. T. Reiss, D. G. Gee, K. Gotimer, L. Q. Uddin, S. H. Lee, D. S. Margulies, A. K. Roy, B. B. Biswal, E. Petkova, F. X. Castellanos and M. P. Milham, The resting brain: Unconstrained yet reliable, *Cerebral Cortex* **19**(10) (2009) 2209–2229.
35. G. L. Shulman, J. A. Fiez, M. Corbetta, R. L. Buckner, F. M. Miezin, M. E. Raichle and S. E. Petersen, Common Blood Flow Changes across Visual Tasks: II. Decreases in Cerebral Cortex, *Journal of Cognitive Neuroscience* **9**(5) (1997) 648–663.
36. S. Smith, P. Fox, K. Miller, D. Glahn, M. Fox, C. M. E., N. Filippini, K. Watkins, R. Toro, A. Laird and C. Beckmann, Correspondence of the brain's functional architecture during activation and rest, *Proceedings of the National Academy of Sciences* **106**(31) (2009) 13040–13045.
37. F. T. Sun, L. M. Miller and M. D. Esposito, Measuring interregional functional connectivity using coherence and partial coherence analyses of fmri data, *NeuroImage* **21**

(2004) 647–658.
38. P.-N. Tan, M. Steinbach and V. Kumar, *Introduction to Data Mining* (Addison-Wesley Longman Publishing Co., Inc., Boston, MA, USA, 2005).
39. M. E. Tipping, Sparse Bayesian Learning and the Relevance Vector Machine, *Journal of Mach. Learn. Research* **1** (2001) 211–244.
40. L. Uddin, A. M. C. Kelly, B. B. Biswal, F. X. Castellanos and M. P. Milham, Functional connectivity of default mode network components: Correlation, anticorrelation, and causality, *Human Brain Mapping* **30**(2) (2009) 625–637.
41. M. van den Heuvel, R. Mandl and H. H. Pol, Normalized Cut Group Clustering of Resting-State fMRI Data, *PLoS ONE* **3** (2008) p. e2001.
42. I. M. Veer, C. Beckmann, M.-J. V. Tol, L. Ferrarini, J. Milles, D. Veltman, A. Aleman, M. V. Buchem, N. V. D. Wee and S. Rombouts, Whole brain resting-state analysis reveals decreased functional connectivity in major depression, *Frontiers in Systems Neuroscience* **4** (2010) p. 41.
43. A. Venkataraman, K. V. Dijk, R. L. Buckner and P. Golland, Exploring functional connectivity in fmri via clustering, *IEEE Intern. Conf. on Acoustics, Speech, and Signal Processing* (2009) 441–444.
44. R. C. Welsh, L. M. Jelsone-Swain and B. R. Foerster, The utility of independent component analysis and machine learning in the identification of the amyotrophic lateral sclerosis diseased brain, *Frontiers in Human Neuroscience* **7** (2013) 30–38.
45. S. Zhao, J. Han, J. Lv, X. Jiang, X. Hu, Y. Zhao, B. Ge, L. Guo and T. Liu, Supervised dictionary learning for inferring concurrent brain networks, *IEEE Transactions on Medical Imaging* **34** (Oct 2015) 2036–2045.
46. H. Zhu, X. Pan and Q. Xie, Merging student's-t and rayleigh distributions regression mixture model for clustering time-series, *Neurocomputing* **266** (2017) 247 – 262.